View Online / Journal Homepage / Table of Contents for this issue
Dynamic Article Links

Energy & Environmental Science

Cite this: *Energy Environ. Sci.*, 2011, **4**, 4882

www.rsc.org/ees

PERSPECTIVE

Magnesium nanocrystal-polymer composites: A new platform for designer hydrogen storage materials

Rizia Bardhan, Anne M. Ruminski, Alyssa Brand and Jeffrey J. Urban*

Received 1st August 2011, Accepted 26th September 2011
DOI: 10.1039/c1ee02258j

Downloaded by Lawrence Berkeley National Laboratory on 11 January 2012
Published on 19 October 2011 on http://pubs.rsc.org | doi:10.1039/C1EE02258J

Metal hydrides, with their inherently high gravimetric and volumetric densities, present a compelling platform for hydrogen storage for mobile applications. However, several fundamental barriers have persistently impeded technological progress. This perspective provides an overview of the current hurdles plaguing metal hydride technology and the novel approaches recently adopted that may potentially surmount these challenges. In particular, nanocomposites, a homogenous matrix of two or more components synergistically integrated for enhanced material performance, is emerging as a new and promising class of material for hydrogen storage. This perspective highlights the potential of nanocomposites, specifically magnesium nanocomposites, for hydrogen storage. First, the existing challenges of metal hydrides are reviewed, followed by the progress achieved thus far by metal hydride size reduction to the nanoscale, and incorporation in a matrix material. Lastly, a novel nanocomposite synthesized by confining magnesium nanocrystals within a gas-selective polymer matrix is highlighted and the potential for improvement is discussed. This metal-polymer nanocomposite holds great promise as a general approach for future work on hydrogen-storage composites, as it simultaneously provides air-stability, high hydrogen storage density, and rapid hydrogenation kinetics.

1. Introduction

Despite prodigious efforts in the search for alternative energy sources, fossil fuels such as coal, oil, and natural gas remain the mainstay of our current energy sources. In response to rapidly depleting fossil fuels, increasing oil prices, and emerging ecological concerns with CO_2 emissions, innovative approaches for energy are imperative for both stationary and mobile applications. Recently, several scientific goals have been promulgated by The U.S. Department of Energy (DOE) in an attempt to guide the transition to a renewable energy platform. These goals include improvement of existing technologies such as fuel cells and batteries, and development of novel strategies to ultimately adapt to a cleaner and abundant energy source.[3,4] Although research in batteries is developing rapidly,[5,6] existing challenges such as low energy density, short lifespan, and complications with regeneration[7] necessitate further research efforts before the full potential of batteries is realized.[8,9] One alternative for transportation purposes is the direct methanol fuel cell (DMFC)

The Molecular Foundry, Materials Sciences Division, Lawrence Berkeley National Laboratory, Berkeley, CA, 94720. E-mail: jjurban@lbl.gov

Broader context

Rapid modernization has catalyzed world energy consumption within the recent decades. To meet this rising energy demand, a transition from carbon-rich fossil fuels to a cleaner and more abundant energy carrier will be necessary to ensure energy security in the future. We have already seen a significant decline in the carbon-to-hydrogen (C:H) ratio in our fuels, and further reduction in the C:H ratio is projected in the next few decades.[1,2] Complete decarbonization of our fuelstocks has been predicted to culminate by 2100 at which time we will have transitioned to carbon-free sources of energy. Among these energy sources, a primary player will be hydrogen, which is not only naturally abundant, but also has minimal environmental impact. However, storing hydrogen within the size and weight limits of a vehicle remains a critical challenge. Solid-state metal hydrides, particularly magnesium hydride, are an exciting substitute to compressed hydrogen tanks, but the practical use of bulk metal hydrides is limited by inaccessible energetics. Nanocomposites, a recently developed class of materials, can be specifically engineered to have superior hydrogen storage properties by selecting appropriate matrix materials. Therefore, in addition to summarizing some of the recent progress in hydrogen storage materials accomplished through nanosizing, this perspective focuses on the promise of nanocomposites as an exciting alternative to the current synthetic approaches for high-capacity hydrogen storage.

 This journal is © The Royal Society of Chemistry 2011

Downloaded by Lawrence Berkeley National Laboratory on 11 January 2012
Published on 19 October 2011 on http://pubs.rsc.org | doi:10.1039/C1EE02258J

which utilizes methanol as a fuel source.[10,11] While DMFCs can provide a potential alternative to batteries,[12] maturity of DMFC technology has been hampered by several drawbacks including high system cost, low operating voltage, low efficiency due to sluggish methanol oxidation reaction, poor durability due to degradation of the Nafion membrane and poisoning of Pt electrocatalysts.[13] Electricity, a major energy carrier, currently dominates the world's energy grid for most mainstream technologies. However, lack of efficient storage options and the high cost associated with power fluctuations and outages limits the use of electricity for future energy needs. Given the sizeable energy challenge facing our economy, H_2 has been identified as a transformational energy carrier ideal for numerous applications.[14,15]

The enormous benefits of H_2 as a sustainable energy carrier have been recognized on account of: (i) it is abundant, primarily in the form of H_2O, (ii) it is a clean energy carrier, the major product of its combustion being H_2O, (iii) it can be generated by simple hydrolysis of H_2O, and more importantly (iv) it has the highest energy density per unit weight compared to non-nuclear fuels.[16,17] For instance, 1 kg of H_2 has the equivalent energy as 3 kg of gasoline, but combustion of gasoline also releases nearly 9 kg of CO_2.[18] A rapid decline in C:H ratio of our fuels has already begun and it is anticipated by 2100 complete transition to a carbon-free fuel source may be accomplished (Fig. 1).[1,2] The potential merits of transitioning to a H_2 economy have sparked phenomenal research efforts on H_2 generation and storage.[18–21] Recent advances in nanomaterials combined with photoelectrochemical cells[22–24] and bio-inspired approaches[25–27] such as hydrogenase-catalyzed biofuel cells[25] or inorganic clusters mimicking hydrogenase[26,27] have improved H_2 production. However, storing H_2 with high efficiency and subsequent release at practical temperatures remains in its infancy owing to lack of promising materials that meet the technical criteria to make them competitive energy carriers.[28] This is largely attributed to fundamental challenges in material development, characterization, and scalability. For instance, the "ideal" market-ready H_2 storage system must simultaneously be: (i) cost-effective, (ii) light-weight and compact, (iii) store a high volumetric density of hydrogen, (iv) have both accessible energetics for activation and low temperature of dissociation, (v) have high stability against moisture and O_2 for extended cycles, (vi) have minimum energy loss during charge and discharge of H_2 and (vii) have a high degree of reversibility. The next section elaborates the specific criteria in further details. Existing H_2 storage systems do not meet all of these requirements, impeding the large-scale production and implementation of H_2-based technologies in the transportation sector.

2. Hydrogen storage materials

2.1 Overview of hydrogen storage options

Conventionally, H_2 is stored in tanks either as a compressed gas or a liquid. However, the safe and practical use of these H_2 storage methods is constrained by the large size of the storage tank, the cost required to liquefy H_2, low volumetric density of H_2, loss of liquid H_2 due to "boil-off" and critical safety concerns due to high pressures involved. Innovations in material development have demonstrated that H_2 can be stored by physisorption on large surface area adsorbents, and in that context, carbon-based nanostructures, metal–organic frameworks (MOFs), zeolites, and polymers with intrinsic microporosity have all been studied extensively as physisorbents.[29–36] While the combination of low mass density, high surface area, and narrow pore sizes are advantageous for H_2 storage in these adsorbents, the cryogenic conditions necessary for loading H_2 and low gravimetric and volumetric densities at practical temperatures are critical drawbacks. Therefore, the technological maturity of these materials for hydrogen storage remains far from commercialization or wider implementation.

Distinct from the microporous adsorbents described above which physically adsorb hydrogen, hydrides of some metals and non-metals form a different class of materials for H_2 storage characterized by their ability to store larger amounts of H_2 through the formation of chemical bonds. A plot of gravimetric density *versus* H_2 release temperature of various bulk metal hydrides is represented in Fig. 2. DOE has set ultimate targets for gravimetric capacity of >9 wt % (hydride weight), volumetric capacity of >80 g L^{-1}, and min/max delivery temperatures of -40 to 85 °C.[37] The delivery temperature of existing solid-state hydrides is very high rendering them ineffective for technological applications. While a few materials have the potential to meet

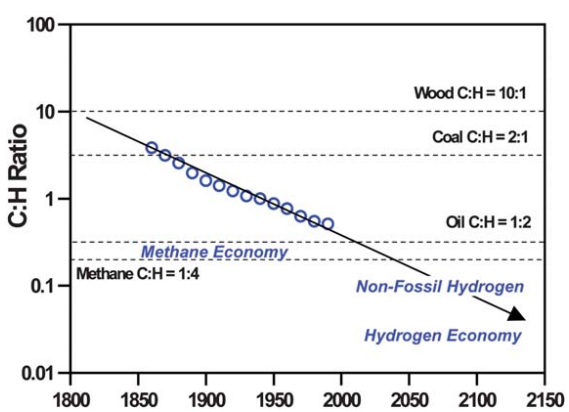

Fig. 1 Decarbonisation evolution in global fuel mix over the course of time. Reprinted with permission from ref. 2, copyright 2007, Australian Petroleum Production & Exploration Association.

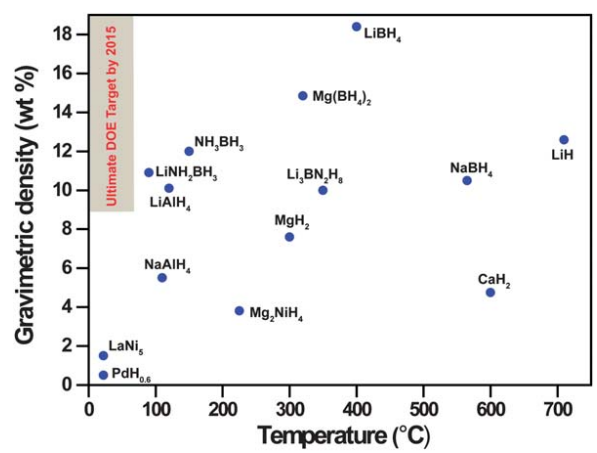

Fig. 2 Hydrogen thermodynamic release temperature (at 1 bar H_2) as a function of gravimetric density of various bulk metal hydrides. The ultimate DOE target to be achieved by 2015 is represented in gray.

Downloaded by Lawrence Berkeley National Laboratory on 11 January 2012
Published on 19 October 2011 on http://pubs.rsc.org | doi:10.1039/C1EE02258J

these targets such as $LiAlH_4$, NH_3BH_3, and $LiNH_2BH_3$, several concerns remain to be addressed: (i) these three materials have critical problems with on-board regeneration and are not usable as reversible storage options which severely lowers their market potential, (ii) they also suffer from poor stability, and in the case of the latter two, generate toxic ammonia and borazine, which is detrimental for fuel cell applications. These limitations will be discussed in more detail in section 3.

It is evident that significant challenges remain to be addressed before the transition from laboratory to commercial setting can be realized with metal hydrides. This perspective will focus on the progress achieved in the past decade with metal hydrides and the existing challenges, in particular for borohydrides $(BH_4)^-$, alanates $(AlH_4)^-$, amineboranes (NH_xBH_x) and amidoboranes $(NH_2BH_3)^-$, and with special emphasis on magnesium hydrides (MgH_2).

2.2 Fundamentals of metal hydrides

The thermodynamic aspects of metal hydride formation are examined through pressure-composition isotherms (Fig. 3). At small hydrogen to metal ratios (H/M $\leq$0.1) below a certain pressure, H_2 is dissolved in the metal as a solid solution (α) phase. As the H_2 concentration increases and pressure rises, the stable metal hydride (β) phase nucleates and grows. While the two phases co-exist, a plateau at constant pressure is observed, the width of which determines the hydrogen storage capacity of the material. The two-phase region ends at a critical temperature (T_C) beyond which the transition from α to β phase is continuous. The plateau pressure correlates to the change in enthalpy (ΔH) and entropy (ΔS) as a function of temperature by the Van't Hoff equation (Fig. 3),

$$\ln\left(\frac{P_{eq}}{P_0}\right) = \frac{\Delta H}{RT} - \frac{\Delta S}{R} \quad (1)$$

While enthalpy determines the strength of the metal-hydrogen bond, entropy corresponds to the change from molecular hydrogen to hydrogen in the hydride phase.

2.3 Applications of metal hydrides

The unique combination of high gravimetric and volumetric density and low production cost of several solid-state hydrides makes them candidate materials for H_2 storage and subsequently for the development of fuel cells for mobile applications.[17,38] Hydrogen-driven fuel cells are already a mature technology currently in use as alkaline fuel cells (AFCs) and proton exchange membrane fuel cells (PEMFCs). In these fuel cells, H_2 undergoes a combustion reaction with O_2 to produce electrical energy and H_2O as the sole by-product. While AFCs and PEMFCs have been historically utilized for on-board power in manned spacecraft produced by the National Aeronautics and Space Administration (NASA),[39] their widespread commercialization for vehicular applications has been hindered due to the use of compressed H_2 cylinders as the fuel source and the limitations associated with them, as well as the high cost and poor durability of these fuel cells. Solid-state H_2 fuel cells, where metal hydrides are used as the H_2 carrier, will not only offer improved energy densities but also provide higher efficiency and overall compact size, properties which can potentially revolutionize fuel cell technology for mobile applications.[40,41] Metal hydride fuel cells can also demonstrate superior performance to batteries, which currently dominate most stationary and portable electronics applications. For instance, AlH_3 fuel cells, which have an energy density of 1200 Wh L^{-1}, are four times higher in energy density than Li polymer batteries, ten times higher than Ni-metal hydride and Ni-Cd batteries and thirty times greater than Pb–acid batteries.[18]

2.4 Importance of nanocomposite materials

Given the tremendous potential of metal hydrides in facilitating the transition to a H_2 economy, in this perspective we focus on the recent progress made in metal hydride technology in the last decade specifically in magnesium (Mg). In particular, we emphasize the significant role of nanocomposites in hydrogen storage applications. While metal hydrides mixed with additives or ball-milled with catalysts have shown some improvement in material properties, historical progress in metal hydrides indicates[42–44] that even skillfully-processed single-phase solids do not simultaneously satisfy all criteria for efficient H_2 storage and that a conceptual match of several properties is needed. In this context, *composites* are highly desirable for enhancing material characteristics. Composites have recently emerged as a new class of material which can be broadly defined as a homogenous matrix of two or more individual constituents which are

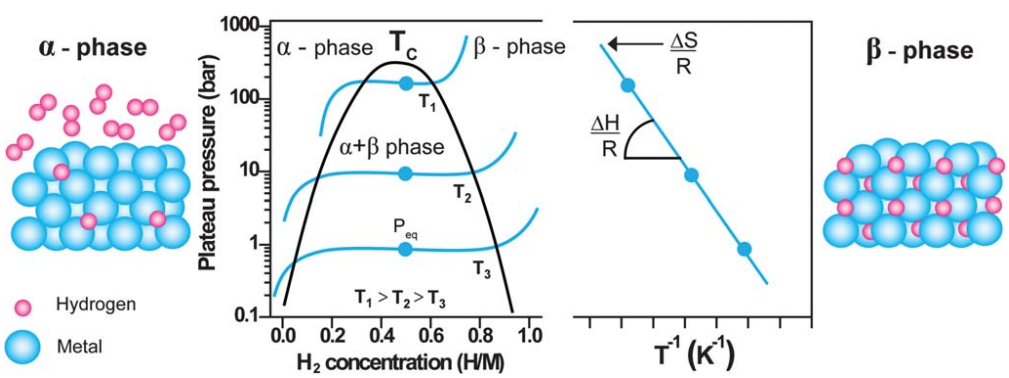

Fig. 3 (Left) Pressure-composition isotherm plot of metal to metal hydride phase transition. (Right) Van't Hoff plot related to the phase transition from metal to metal hydride. The enthalpy and entropy of hydride formation and decomposition is obtained from the slope and intercept, respectively. Schematic representation of α-phase (left) and β-phase (right) of metal hydride are also shown.

 This journal is © The Royal Society of Chemistry 2011

Downloaded by Lawrence Berkeley National Laboratory on 11 January 2012
Published on 19 October 2011 on http://pubs.rsc.org | doi:10.1039/C1EE02258J

synergistically integrated to achieve an optimum design and performance unattainable by the individual components.[45] In particular, to intelligently design nanocomposites several criteria need to be considered: (i) the properties of the host matrix should reciprocate with the characteristics of the nanoparticles that are incorporated, (ii) appropriate synthetic strategies should be adapted to ensure uniform distribution of nanoparticles in the host matrix, and (iii) the nanocomposite should demonstrate enhanced capabilities without compromising the existing merits of individual constituents. Nanocomposites where nanomaterials are incorporated with polymers or porous carbon structures, have recently piqued significant interest attributed to their superior optical, electrical, mechanical and gas-sensing properties.[46] Nanocomposites have recently been applied in a range of technologies from fuel cells to aircraft structures and are expected to substantially accelerate the field of hydrogen storage as well.

Extensive research efforts, some of which will be discussed in the next section, have demonstrated that nanostructuring, nanoconfinement and formation of nanocomposites give rise to increased specific surface area, as well as increased concentration of defects, steps, and corner atoms, which likely controls the association and dissociation of H_2.[47] Collectively these effects result in (i) enhanced kinetics attributed to the shorter diffusion lengths for H_2 and possibly higher nucleation rates due to nucleation occurring on the surface of nanostructured materials, (ii) better reversibility, (iii) improved mechanical and thermal stability during cycling specifically if carbon materials are added to the system, and (iv) improved thermodynamics due to destabilization of the hydride phase.[47,48] It must be noted, however, size reduction can also result in stabilization of the hydride phase for some metal hydrides (VH_2, LiH, TiH_2, AlH_3) as shown by Sholl *et al.*[49] This is correlated to the volume-adjusted surface energy difference as the metal converts to its hydride phase given by

$$3V_M\Delta_{M\rightarrow MH_2(\gamma,r)} = \left[\gamma_{MH_2}(r)\left(\frac{V_{MH_2}}{V_M}\right)^{2/3} - \gamma_M(r)\right] + E_{ads} \quad (2)$$

If the surface energy of the metal hydride phase, $\gamma_{MH2}(r)$, is larger than that of the metal, $\gamma_M(r)$, size reduction results in thermodynamic destabilization of the hydride phase, while stabilization of the hydride phase is observed if the surface energy of the metal is higher. Since the surface energy for most metal hydrides has not been examined experimentally, many of the size-induced thermodynamic effects that have been suggested remain mostly speculative. A more detailed understanding of size-effects is discussed in extensive reviews by Aguey-Zinsou *et al.*,[50] Berube *et al.*,[48] and de Jongh *et al.*[47] and will not be reiterated here due to the scope of this Perspective.

In the next section we discuss the progress in metal hydrides focusing on the importance of nanocomposites and nanosizing. We specifically highlight our recent work on Mg-polymer nanocomposites[51] which combine the unique features of air-stability, high storage capacity, and low activation energies (E_A) relative to bulk Mg. We also discuss future perspectives on understanding the fundamental properties of this material for technological applications. Additionally, we emphasize the advancements made with MgH_2, current technological challenges, the promise of nanosizing and nanoconfinement in surpassing these barriers and future endeavors necessary for practical use of MgH_2 with fuel cells.

3. Recent progress in metal hydrides and ongoing challenges

Two decades ago transition metal-based hydrides were central to the research dedicated to H_2 storage, however, low storage capacities owing to their high atomic weights impeded their practical use.[52] Recent studies have demonstrated that hydrides based on light elements (Li, Na, Be, Mg, Ca, B, N and Al) may provide the desired H_2 storage content necessary for large-scale commercialization, and are briefly discussed in this section.

3.1 Borohydrides

Borohydrides $(BH_4)^-$ of the alkali and alkali-earth metals are of particular interest due to their high gravimetric and volumetric densities. For example, lithium borohydride ($LiBH_4$) has a storage capacity of 18 wt% H_2. However, the high temperature (~400 °C at 1 bar) required to release H_2 from $LiBH_4$ severely diminishes the practical relevance of this material.[53] Additionally, volatile boranes are often released as by-products which results in loss of storage capacity over multiple cycles. Recent advances have demonstrated that the use of additives or catalysts can destabilize the hydride phase, thereby reducing the desorption temperature. For instance, the dehydriding temperature of $LiBH_4$ mixed with MgH_2 was significantly lowered to 225 °C at 1 bar and a dehydrogenation enthalpy of 40.5 kJ mol^{-1} was obtained compared to a pure $LiBH_4$ enthalpy of ~65 kJ mol^{-1}.[53] There is experimental evidence, however, that size reduction of the crystal domains to the nanoscale may also decrease the dehydrogenation enthalpy and enhance the kinetics of absorption and desorption.[53–60] Recently, thermodynamic destabilization was achieved for $LiBH_4$ nanoparticles supported by disordered mesoporous carbon, where nanosizing facilitated "thermal stable tailoring" of $LiBH_4$ as well as diffusion and recombination of segregated LiH and B phases when H_2 was charged.[61] In addition to improved thermodynamics, nanosizing also augments kinetics, for instance, enhanced kinetic rates and a reduced dehydrogenation temperature were observed for $LiBH_4/MgH_2$ mixtures confined within nanoporous carbon aerogels.[54] Likewise, nanocomposites of $LiBH_4$ encapsulated within a 13 nm diameter pore-size carbon scaffold decreased desorption E_A from 146 kJ mol^{-1} to 103 kJ mol^{-1} and increased kinetic rates by 50 times relative to bulk.[55] Furthermore by replacing carbon scaffolds with carbon nanotubes of only 2 nm diameter, the E_A of $LiBH_4$ was remarkably reduced to 88 kJ mol^{-1}.[56] These examples exemplify the merits of nanocomposite formation for improving the energetics of H_2 storage and release in borohydrides.

3.2 Alanates

Alanates $(AlH_4)^-$, similar to borohydrides, also form a class of complex hydrides with high gravimetric and volumetric densities. Sodium alanate ($NaAlH_4$), for example, can release 5.6 wt% H_2 in a two-step reaction,

Downloaded by Lawrence Berkeley National Laboratory on 11 January 2012
Published on 19 October 2011 on http://pubs.rsc.org | doi:10.1039/C1EE02258J

$$3NaAlH_4 \rightarrow Na_3AlH_6 + 2Al + 3H_2 \quad (3)$$

$$Na_3AlH_6 \rightarrow 3NaH + Al + 3/2\ H_2 \quad (4)$$

At ambient pressure, the equilibrium temperatures for the above two steps for bulk $NaAlH_4$ are estimated to be 30 °C and 130 °C, respectively. Despite the lower decomposition temperatures, slow kinetics and poor reversibility have obstructed the progress of this material as a functional fuel source.[19] A recent work demonstrated that nanocomposites of $NaAlH_4$ with carbon nanofibers produced 2–10 nm diameter particles that exhibited a reduction in desorption temperature and E_A from 186 °C and 116 kJ mol^{-1} for bulk to 70 °C and 58 kJ mol^{-1}.[62] Calculations further predicted that $NaAlH_4$ particle sizes ≤10 nm decompose in a single step at temperatures realistic for PEMFCs.[63] Significant changes in thermodynamic properties have also been observed for nanosized $NaAlH_4$ confined in mesoporous (0.4–5 nm pores size) activated carbon fibers[64] and nanoporous carbon material.[65] Size reduction of $NaAlH_4$ to ≤1.5 nm, by confining in MOF scaffolds, also enhanced desorption kinetics and ~80% of stored H_2 was released at a significantly lowered temperature relative to bulk.[66] Additionally, doping with titanium-based compounds[67,68] and carbon-based materials[69] has been shown to effectively improve cyclability of this material. Another member of the alanate family, lithium alanate, has also been investigated for its exceptional gravimetric density of 10.5 wt% H_2. However, the thermodynamics and kinetics of lithium alanate is less favorable compared to sodium alanate. Current research efforts are focused on either destabilization of $LiAlH_4$ to improve kinetics and reversibility, for example by doping with nanocrystalline MgH_2,[70] or regeneration of $LiAlH_4$ by cost-effective low-energy routes to make them suitable for practical applications.[71] Additionally the potential of rare-earth alanates are also being studied for use in low temperature fuel cells.[72]

3.3 Amineboranes and amidoboranes

Besides alanates and borohydrides, boron-nitrogen compounds have also been examined extensively as promising hydrogen storage media.[73,74] For instance, the amine-borane (NH_xBH_x) family of compounds has theoretical gravimetric densities of 24.5, 19.6, 14, and 7.5 wt% H_2 for x = 4, 3, 2, and 1, respectively, and low decomposition temperatures of ~120 °C.[75] Amine-borane and its derivatives release hydrogen variously by thermally-induced, acid-induced, and/or metal catalyst induced solvolysis. Despite the high storage capacities, the issues of poor reversibility, slow kinetics at low temperatures (≤85 °C), excessive borazine and ammonia formation and energy-intensive procedures required to regenerate amineboranes are major drawbacks that must be addressed before realistic goals are achieved with this class of materials.[76] Recent advances in nanocomposites such as loading amine-borane in nanochanneled silica scaffolds[77] and nanoporous carbon cryogels[78] exemplified that nanocomposites provides a route to further enhance these materials and overcome many of the aforementioned disadvantages. Furthermore, the use of monometallic[79–81] and bimetallic[82,83] nanoparticle catalysts as well as nanoscale additives[84] has also produced improved kinetics and thermodynamics of H_2 release by ammonia borane.

An alternative approach to manipulating the energetics of ammonia boranes is through chemical alteration by substituting one protic H in the NH_3 group with an electron-donating metal.[85] Lithium ($LiNH_2BH_3$) and sodium amidoboranes ($NaNH_2BH_3$) have demonstrated high gravimetric densities of 10.9 wt.% and 7.5 wt.% respectively and accessible dehydrogenation temperatures (90 °C).[86] In addition, dehydrogenation is less exothermic compared to ammonia borane. $LiNH_2BH_3$ was also shown to release two equivalents of hydrogen at temperatures as low as 40 °C when dissolved in tetrahydrofuran demonstrating the promise of these materials for future energy needs.[87] However, formation of ammonia remains an issue with amidoboranes which is severely detrimental for fuel cell membranes.

3.4 Magnesium hydrides

The promise of magnesium (Mg) as a candidate material for H_2 storage was examined as early as the 1960's.[88] With its high storage capacity of 7.6 wt %, high volumetric capacity of 110 g L^{-1}, earth abundance, low cost and highest known energy density of all reversible hydrides (9 MJ kg^{-1} Mg), Mg is highly desirable for on-board H_2 storage. Despite the immense merits of Mg, several challenges have hampered the growth of magnesium hydrides (MgH_2) for fuel cell applications. Mg converts to its corresponding hydride (β-MgH_2) by dissociation of the H_2 molecules on the activated metal surface and further diffusion of H atoms into the bulk. Although diffusion is not the limiting step initially, as the reaction proceeds a nearly impermeable hydride layer is formed. Diffusion through this hydride layer thus later becomes the rate-limiting step resulting in slow kinetics of hydride formation and decomposition. The sluggish kinetics is also partially attributed to rapid oxidation of magnesium, which produces a magnesium oxide (MgO) surface layer that is nearly H_2-impermeable, thus severely impeding further transformation. Additionally, due to the high thermodynamic stability of MgH_2, the enthalpy and entropy of bulk magnesium hydride decomposition are 75 kJ mol^{-1} H_2 and 130 J K^{-1} mol^{-1} H_2. Furthermore, temperatures in excess of 300 °C are required for complete dehydridation of MgH_2, nearly 3 times higher than the operational temperature of PEM fuel cells. Recent research efforts have thus been focused on reducing the thermodynamic stability of MgH_2, improving the stability of Mg towards oxygen and moisture, and enhancing hydriding and dehydriding kinetics. Several approaches have been adopted including: (i) alloying or doping with transition metals, (ii) use of borohydrides and alanates as additives, (iii) nanoscaling the Mg crystal size and (iv) forming nanocomposites with carbon scaffolds.

Theoretical investigations have recently indicated that decreasing the cluster size of MgH_2 to <1 nm can destabilize the hydride phase substantially, as desired.[89,90] This size reduction is calculated to decrease the desorption enthalpy to as low as 63 kJ mol^{-1} H_2 with a corresponding desorption temperature of 200 °C.[89] Simulations have also predicted that appropriate amounts of dopants such as Li[91] and transition metals,[92] or alloying with Ti-Al/Si can remarkably destabilize the hydride phase as well.[93] Mg-Ti-Si and Mg-Ti-Al alloys can potentially

 This journal is © The Royal Society of Chemistry 2011

Downloaded by Lawrence Berkeley National Laboratory on 11 January 2012
Published on 19 October 2011 on http://pubs.rsc.org | doi:10.1039/C1EE02258J

lower the hydrogenation energies to a range (39 to 48 kJ mol^{-1} H_2) suitable for most commercial applications.[93] These calculations correlate well with experiments which show that dehydrogenation of Mg_xTi_yAl/Si_{1-x-y} thin films occur at a higher plateau pressure (indicating destabilized hydride phase) compared to Mg films alloyed with Ti only.[94] Computations have also concluded that mixing borohydrides and amides such as $LiBH_4$ and $LiNH_2$,[95] and a spill-over mechanism initiated by capping Mg films with Pd,[96] also contributes to improved thermodynamic and kinetic properties in Mg.

Calculations have indicated that metal catalysts, whether co-doped in small quantities, alloyed, or mixed as an additive, can promote improved energetics of H_2 sorption in Mg.[92] Catalysts comprised of transition metals (Fe, Nb, Ni, Zr, Cr, Ti, V, Fe, Pd, Cu, Co, Rh),[97–102] oxides of transition metals,[103] halides of transition metals (Cl, F),[104] and semiconductors (Si)[105] have been computationally shown to be effective. Catalysts increase the rate of dissociation of H_2 molecules on the Mg surface, thereby creating mobile H atoms which can result in faster rates of diffusion into the Mg crystal lattice. This results in enhanced kinetics of hydrogenation, lower desorption temperatures and higher H concentrations chemisorbed in Mg.[101] For instance, nanocrystalline domains of Fe were also shown to catalytically promote H_2 absorption near room temperature and significantly lower desorption temperatures (130–250 °C). In addition to catalysts, reactive mixtures of borohydrides, alanates, and amides with MgH_2 termed as "reactive hydride composites" also improve the kinetics.[106–108] Yang *et al.* recently demonstrated a "self-catalyzing" strategy by mixing $LiBH_4/LiNH_2$ with MgH_2 which yields product nuclei for a subsequent reaction resulting in an overall improved reversibility, faster kinetics and lower desorption temperature.[107]

The insights afforded by calculations have provided ample motivation for researchers to develop Mg nanostructures, and indeed a vast literature of work has emerged within the last decade. Nanoscale Mg exhibits properties far superior than that achieved by catalyst doping of bulk Mg alone. Various synthetic routes have been adopted such as mechanochemical milling,[109] organometallic chemistry,[110,111] solution-processing using colloidal chemistry,[112–114] sonoelectrochemistry,[115] and gas-phase methods[116–118] which produce Mg/MgH_2 particles from ~3 nm to the sub-micron scale. To highlight one such effort, Mg nanowires in the size range of 30–170 nm were synthesized by a vapor-transport approach.[116] Size dependent H_2 absorption/desorption studies demonstrated that smallest diameter nanowires absorbed ~5.8 wt% H_2 and desorbed ~3 wt% in 30 min at 200 °C relative to the largest diameter wires which absorbed ~3 wt% and desorbed only 0.5 wt% (Fig. 4). A theoretical study later predicted a desorption enthalpy of 34.5 kJ mol^{-1} H_2 when wire diameters were reduced to 0.85 nm.[119] Theory also elucidated that H atoms, which are initially located in tetrahedral holes where the H atom is 4-fold-coordinated, migrated to surface bridge sites during hydriding where the H atom is double-coordinated (Fig. 5). Following this work, Mg nanocolloids of 5 nm were synthesized by wet-chemical approaches, and exhibited reversible H_2 storage of 7.6 wt% H_2 at 85 °C.[112] Mg nanoparticles of 2–3 nm diameter

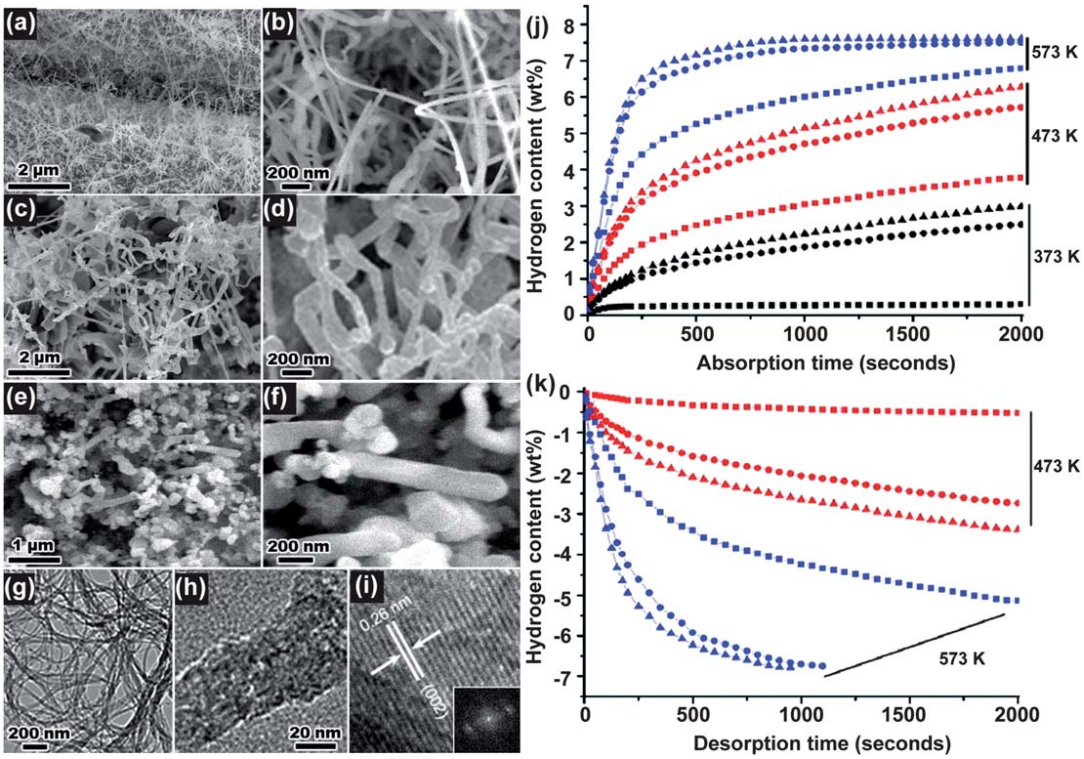

Fig. 4 SEM images of Mg nanowires of diameters (a, b) 30–50 nm, (c, d) 80–100 nm and (e, f) 150–170 nm. TEM (g, h), and HRTEM (i) images of smallest diameter nanowires with the corresponding fast Fourier transform (FFT) pattern (inset). Hydrogen absorption (j) and desorption (k) of the Mg nanowires of various diameters indicated with different symbols (30–50 nm, triangle; 80–100 nm, circle; 150–170 nm, square) at different temperatures (373 K, black; 473 K, red; 573 K, blue). Reprinted with permission from ref. 116, copyright 2007, American Chemical Society.

Downloaded by Lawrence Berkeley National Laboratory on 11 January 2012
Published on 19 October 2011 on http://pubs.rsc.org | doi:10.1039/C1EE02258J

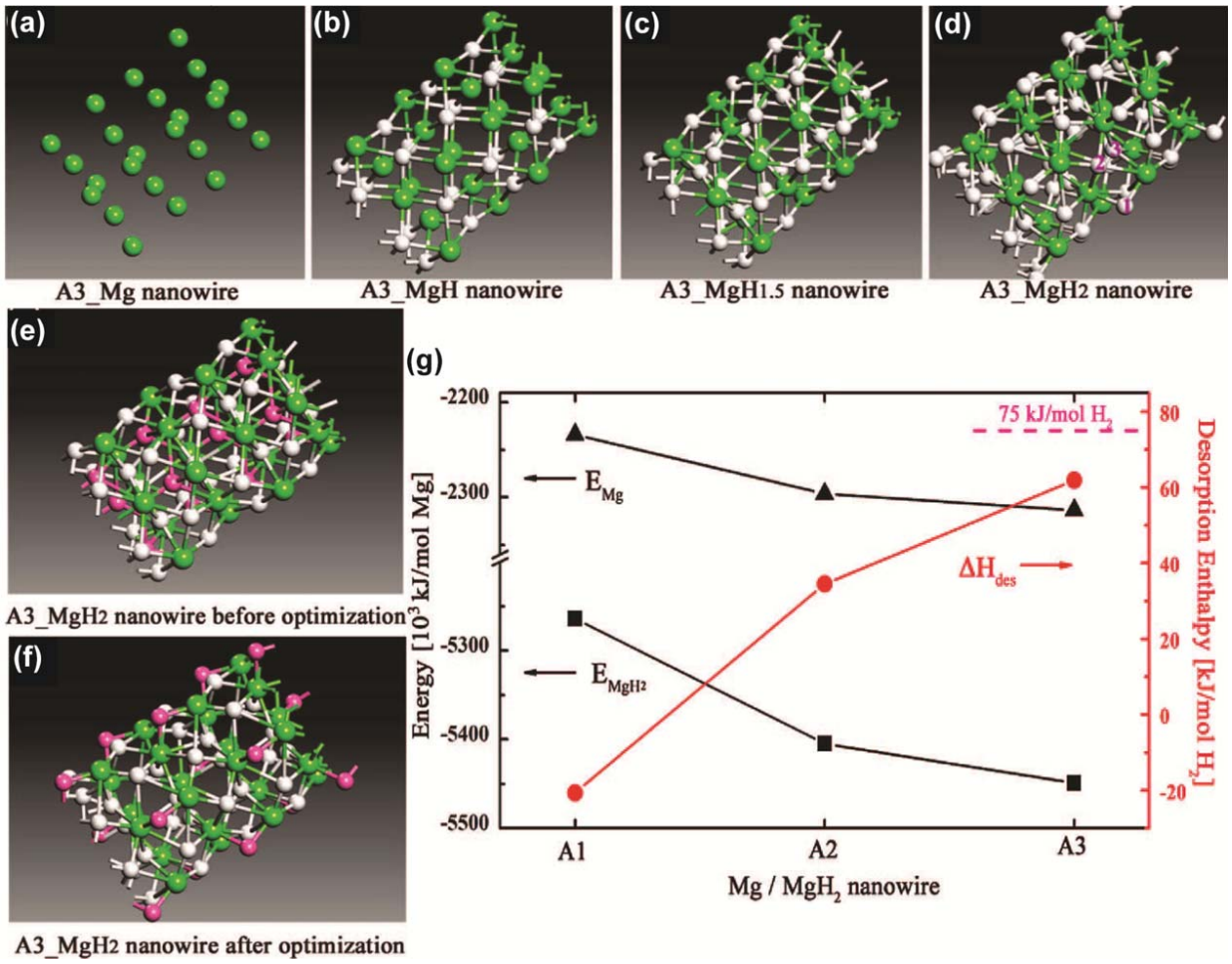

Fig. 5 Hydrogenation process simulated for 1.24 nm diameter Mg nanowire: (a) Mg nanowire, (b) MgH nanowire, (c) $MgH_{1.5}$ nanowire, and (d) MgH_2 nanowire. The structures of MgH_2 (e) before optimization showing H atoms located in tetrahedral holes where the hydrogen atom is 4-fold-coordinated and (f) after optimization showing H atoms diffused to surface bridge site where the H atom is double-coordinated, indicating that H atoms tend to expose to the surface. (g) Desorption enthalpy for MgH_2 nanowires (red line) and the size effect of the calculated energies for magnesium (triangle) and MgH_2 (square) nanowires. The desorption enthalpy are normalized per mol of H_2 released and the energies are normalized per Mg/MgH_2 unit. Reprinted with permission from ref. 119, copyright 2009, American Chemical Society.

were also reported which showed a dehydriding onset temperature of 115 °C.[113] While the low desorption onset temperature is compelling, the majority of desorption still occurred >350 °C which was attributed to sintering of nanoparticles due to ligand removal at elevated temperatures. Recently, Mg nanoparticles between 25 and 38 nm were also systematically evaluated and an improvement in kinetics of hydriding and dehydriding was observed with decreasing particle size (Fig. 6).[114] Nevertheless, temperatures ≥335 °C were still required for desorption. It is interesting that although theoretical predictions indicate that size reduction to <1 nm is necessary for hydride phase destabilization, the recent experimental observations mentioned above distinctly show that significant improvement in properties can be attained at much larger particle sizes. These observations would indicate that in addition to size, factors such as surface energy, material interfaces, and crystallographic planes may also contribute to the overall H_2 storage performance.[50] It is important to note that without thorough experimental investigations in smaller size ranges, which currently do not exist, it would be difficult to provide a definitive explanation for disparities between experiment and theory. A detailed size- and shape-dependent experimental study of particles with dimensions <5 nm is essential to elucidate these effects. Additionally, it is important to note, theoretical predictions largely rely on the surface energies assumed for calculations and may not account for the steps, kinks, edges, corners, and defects generated in nanocrystals with decreasing size, which can potentially contribute to the discrepancy in theory and experimental results reported thus far.

The properties of Mg can be further improved by mixing with carbon nanostructures[120–122] as structural additives. For example, MgH_2 mixed with carbon nanofibers of various geometries (planar, helical and twisted) showed ~5 wt% H_2 absorption with twisted carbon nanofibers within 15 min at 300 °C compared to ~3 wt% for pure Mg. The activation energy of absorption was also observed to reduce by 33 kJ mol^{-1} H_2 when twisted carbon nanofibers were added.[120] MgH_2-single walled carbon nanotube mixtures also exhibited lower E_A of desorption and increased stability over multiple cycles compared to bulk MgH_2.[122] An exciting alternative approach to improving characteristics is by

 This journal is © The Royal Society of Chemistry 2011

Downloaded by Lawrence Berkeley National Laboratory on 11 January 2012
Published on 19 October 2011 on http://pubs.rsc.org | doi:10.1039/C1EE02258J

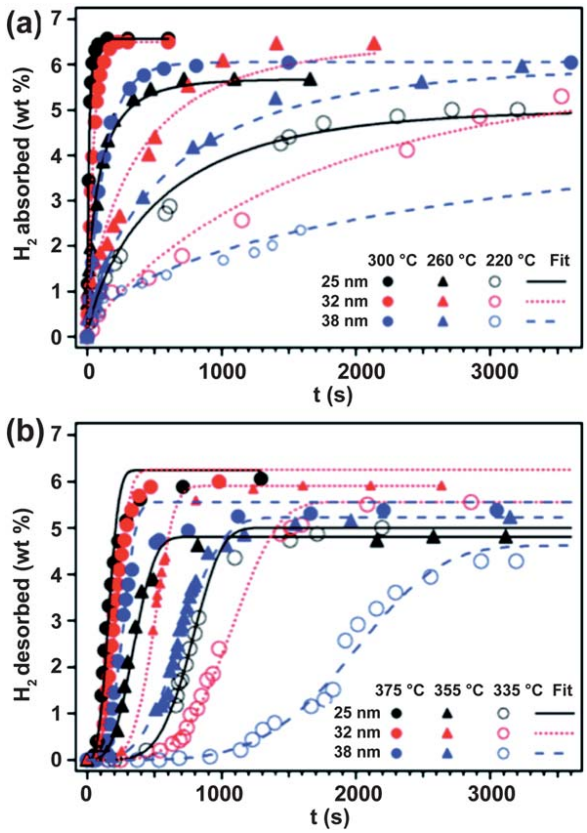

Fig. 6 H_2 absorption (a) and desorption (b) of Mg nanocrystals of various sizes at different temperatures. Reprinted with permission from ref.114, copyright 2011, American Chemical Society.

formation of nanocomposites by incorporating Mg within nanoporous carbon aerogels and other porous carbon structures.[123–127] De Jongh *et al.* systematically examined the efficient loading of carbon matrices with molten Mg resulting in particle sizes in the range of 2–5 nm.[123] Recently MgH_2 nanoparticles synthesized by confining in carbon aerogels of 7 nm and 22 nm pore size exhibited enhanced dehydriding kinetics relative to their bulk counterparts.[124] MgH_2 nanoparticles when integrated in 13 nm diameter pore carbon frameworks with Ni and Cu catalysts also demonstrated higher desorption rates, 25 wt% h^{-1} with Ni and 5.5 wt% h^{-1} with Cu respectively, compared to 0.12 wt% h^{-1} with MgH_2-graphite mixtures.[125] The enhanced thermodynamics and kinetics of Mg-carbon nanocomposites can be attributed to a combination of size effects and interaction with the carbon material, for example with the terminating groups on the edges of the carbon material.[128]

The progress achieved in the past decade to surmount the inevitable challenges of Mg has been remarkable and with continued efforts the use of MgH_2 in H_2 driven fuel cells may be foreseeable in the future. However, there are several concerns which remain to be resolved before practical applications with Mg can be realized: (i) rapid oxidation of Mg forms MgO (and often $Mg(OH)_2$) passivating layers, which invariably slows the hydrogenation kinetics and decreases the H_2 storage capacity, (ii) catalysts and additives enhance reaction kinetics but compromise gravimetric densities of H_2 in the process, (iii) nanosizing also improves kinetics, however stabilizing ligands on nanoparticle surfaces need to be removed for efficient H_2 diffusion, which often results in sintering and agglomeration and consequent degradation of storage capacity over multiple cycles and (iv) decomposition temperatures are still too high for use in fuel cells (90 °C). It is important to note, however, that nanocomposites have shown remarkable promise in improving H_2 storage properties attributed to the inherent characteristics of a homogenously integrated material. On the contrary, heterogeneous mixtures of constituents such as a mixture of two metal hydrides or metal hydride with catalyst have only demonstrated mediocre improvements in performance. In this context, the next section focuses on our recent efforts in addressing many of the aforementioned challenges by developing a novel nanocrystal-polymer nanocomposite.

4. Addressing challenges with magnesium nanocrystal-polymer composites

Recently we developed a simple, one-pot synthetic route that produced air-stable nanoscale magnesium composites.[51] Conventionally, in most synthetic approaches, nanocrystals are stabilized with a protective ligand to ensure oxidative stability and to keep nanocrystals well-dispersed to prevent agglomeration upon hydrogen cycling. However, ligands impede efficient H_2 gas diffusion resulting in slow H_2 kinetics. Further, ligands (or porous frameworks used as size-directing materials) add weight to the material, reducing the overall hydrogen gravimetric density of the system. In an effort to minimize these drawbacks, we adopted a solution-processed approach and directly synthesized Mg nanocrystals within a gas-selective polymer matrix. Through this method the nanocrystals were effectively covered with a minimal amount of polymer, resulting in air stability and preventing agglomeration. Moreover, it was important to have a flexible polymer that could withstand the volume expansion (~33% incurred by the transition of Mg to MgH_2). The polymer poly(methyl methacrylate) (PMMA) was chosen due to its high hydrogen gas selectivity, having a H_2/O_2 permeability ratio of 42.9 at 35 °C. Thus, the Mg nanocrystals were encapsulated in a polymer matrix ligand that has minimal impact on H_2 gas diffusion.

The Mg-PMMA nanocomposites were synthesized through a Rieke-like metal reduction at room temperature under inert atmosphere from a tetrahydrofuran (THF) solution containing dissolved PMMA (M_w = 120,000), bis(cyclopentadienyl) magnesium (Cp_2Mg, the organometallic precursor), and lithium naphthalide (the reducing agent).[51,129,130] Magnesium nanocrystals form through the burst-nucleation and growth mechanism that is well-established in the colloidal nanocrystal community. We posit that the PMMA behaves as both the surface capping agent and the stabilizing ligand. This ensures that the magnesium nanocrystals have a smooth and coherent interface with PMMA, which is required for long-term air-stability to be realized.

Transmission electron microscope (TEM) images presented 4.9 ± 2.1 nm diameter spherical magnesium particles dispersed in the polymer matrix without agglomeration (Fig. 7a). Digital diffractograms of TEM images taken of Mg-PMMA nanocomposites after 2 weeks of air exposure displayed diffraction from solely hexagonal crystalline magnesium; no oxidized

Downloaded by Lawrence Berkeley National Laboratory on 11 January 2012
Published on 19 October 2011 on http://pubs.rsc.org | doi:10.1039/C1EE02258J

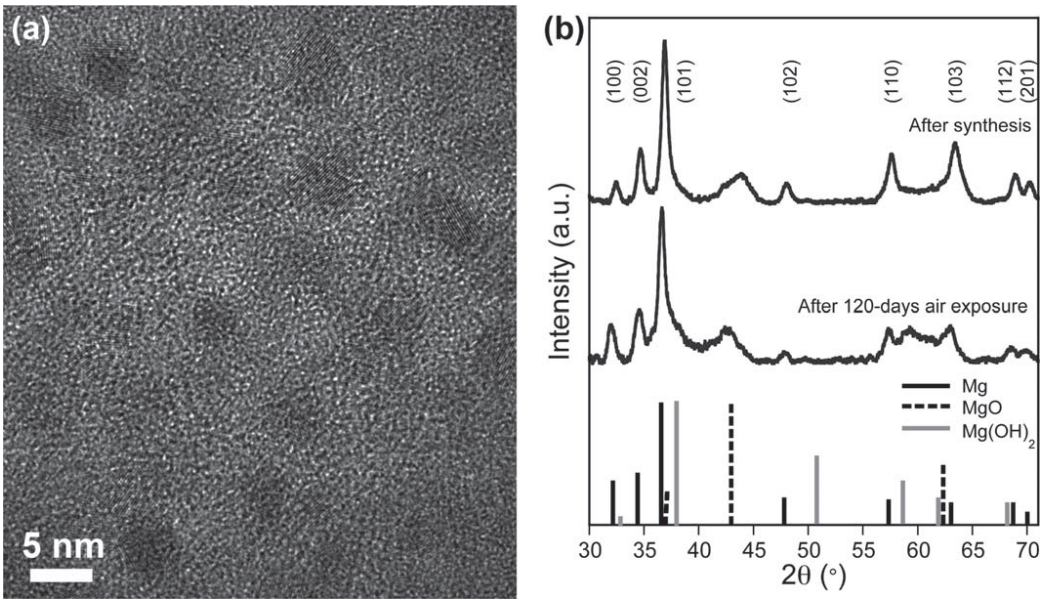

Fig. 7 (a) Transmission electron microscope image of the Mg-PMMA composite, revealing an average Mg nanocrystal diameter of 4.9 ± 2.1 nm. Adapted with permission from ref. 44 copyright 2011, Nature Publishing Group. (b) X-ray diffraction patterns of the Mg-PMMA nanocomposite (top) after synthesis and (middle) after air exposure for 120 days, displaying peaks corresponding well with the (bottom) hexagonal Mg reference pattern (solid black line, JCPDS 04-0770). For comparison, oxide reference patterns of cubic MgO (dashed black line, JCPDS 89-7746) and hexagonal $Mg(OH)_2$ (pale grey line, JCPDS 07-0239) are included.

magnesium was detected. Additionally, X-ray diffraction (XRD) patterns of Mg-PMMA nanocomposites taken immediately after synthesis and after 120 days of air exposure exhibited diffraction peaks characteristic of single-phase hexagonal magnesium and exceptionally minute intensity peaks characteristic of $Mg(OH)_2$ and MgO (Fig. 7b), indicating impressive air stability. Thermogravimetric analysis attributed 61 wt% of the Mg-PMMA composite to Mg, equating to an overall composite theoretical hydrogen gravimetric density of 4.7 wt%.

The H_2 storage capacity of the nanocomposites was examined by using a Sieverts-type reactor (PCT Pro-2000, Hy-Energy). The absorption/desorption tests were performed at 200 °C and 35 and 0 bar of H_2, respectively. Upon hydrogen exposure, the Mg-PMMA nanocomposites exhibited a sharp increase in weight for the initial 6 min followed by a plateau to a constant weight in <30 min (Fig. 8a). The difference in slope is attributed to a change in the rate-limiting mechanism for hydrogen absorption.[131] The experimental hydrogen storage capacity was 5.97 wt% Mg, equating to ~4 wt% for the overall composite. For comparison, a bulk Mg (44 μm) reference material was hydrogenated following the same procedure. Unlike the nanocomposites, the bulk Mg showed no weight increase on hydrogen exposure indicating a lack of hydrogen absorption at 200 °C and 35 bar. The preservation of hydrogen storage capacity of the Mg-PMMA nanocomposites over multiple absorption/desorption cycles was analyzed. The capacity was maintained throughout three full cycles, however, full hydrogen desorption during cycling was not reached, garnering a reversible hydrogen capacity of 3.8 wt% Mg (2.3 wt% in overall composite mass). Additionally, the slope of dehydrogenation of the third cycle was reduced (Fig. 8a inset) indicating slower dehydriding kinetics.

As discussed earlier, nanoscale particle size has been shown to enhance kinetics relative to bulk Mg. Therefore, it was pertinent to measure the activation energy of hydrogen absorption and desorption in the Mg-PMMA nanocomposites. The absorption and desorption of hydrogen at three different temperatures (200, 250, and 300 °C) was analyzed following the procedure detailed above. The hydriding and dehydriding curves display an exponential decay with time; the time constant of these exponentials can be fit to an Arrhenius form $\left[\ln(k) = -\frac{E_A}{R}\frac{1}{T} + \ln(A)\right]$, where k is the reaction rate, A is a temperature independent coefficient, R is the gas constant, and T is the temperature in Kelvin, yielding activation energy, E_A, of absorption and desorption from the slope of the linear fit (Fig. 8b). The E_A of absorption was measured as 24.5 kJ mol^{-1}, and that of desorption as 79.5 kJ mol^{-1}. These recorded values are more than 100 kJ mol^{-1} smaller than the activation energies reported for bulk Mg: 160–200 and 200–240 kJ mol^{-1} for absorption and desorption, respectively.[50]

Mg-PMMA nanocomposites subjected to hydrogen absorption and desorption was reintroduced to ambient atmosphere. X-ray diffraction patterns acquired after 1 month of air exposure displayed peaks characteristic of magnesium with minute intensity peaks from oxidized magnesium. The minuscule MgO peaks observed in XRD suggests that the polymer is sufficiently flexible such that polymer cracking upon volume expansion of the Mg nanocrystals is negligible in this system. Overall, these composites of Mg nanocrystals encapsulated in a gas-selective permeable polymer are simple to synthesize, effectively uptake hydrogen, and show enhanced kinetics through material nano-scaling without suffering degradation or oxidation.

While reproducible synthesis of this material and its properties has been achieved, the fundamental achievable limits of each of the unique properties (*e.g.* density of loading of Mg, uptake and release kinetics, polymer/nanocrystal interfacial gas barrier

 This journal is © The Royal Society of Chemistry 2011

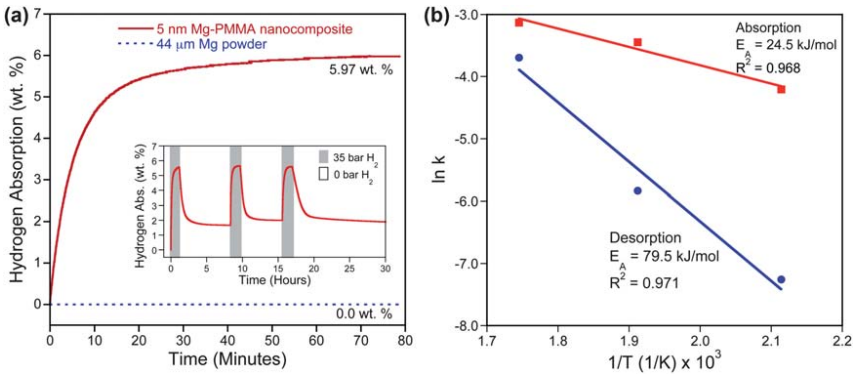

Fig. 8 (a) Hydrogen absorption in Mg-PMMA nanocomposites (red line) at 200 °C and 35 bar shows enhancement in comparison to bulk magnesium powder (blue dashed line). Inset: Hydrogen absorption/desorption cycling in the nanocomposites at 200 °C. The hydrogen absorption capacity was preserved through three full cycles, maintaining an absorption capacity value of 5.97 wt% Mg (~4 wt% in overall composite mass). Not all hydrogen was released upon desorption, resulting in a reversible capacity of 3.8 wt% Mg (2.3 wt% composite). (b) Hydrogen absorption (red squares) and desorption (blue circles) was measured at three temperatures (200, 250, and 300 °C). By plotting the natural log of the rate constant *vs.* inverse temperature (in Kelvin), the activation energy of absorption (24.5 kJ mol^{-1}) and desorption (79.5 kJ mol^{-1}) was determined. Panels adapted with permission from ref. 44 copyright 2011, Nature Publishing Group.

Downloaded by Lawrence Berkeley National Laboratory on 11 January 2012
Published on 19 October 2011 on http://pubs.rsc.org | doi:10.1039/C1EE02258J

properties, *etc.*) of this novel nanocomposite remain unknown. Thus, there exists an enormous opportunity to optimize this material and advance the field of H_2 storage if the fundamental principles of operation can be explored and understood. Moreover, the lessons learned from this Mg-PMMA system may lend crucial insights useful to the design of other classes of nanocrystal-polymer composites for hydrogen storage or gas-capture applications.

5. Future perspectives

There are several properties of the Mg-PMMA nanocomposites that may be optimized in order to improve upon the existing characteristics of the material. Two examples are the Mg loading capacity of the polymer, and the particle size. This goal can be achieved by judiciously balancing the quantity of each reactant such that it does not: (i) increase the particle size, (ii) modify the morphology, (iii) sacrifice the oxidative stability of the composite or (iv) generate byproducts which decrease the overall yield. It is evident, due to the intrinsic limitations of MgH_2, which has a maximum theoretical capacity of 7.6 wt.%, Mg-PMMA nanocomposites will not reach the 2015 DOE target of ≥9 wt.% H_2. Nevertheless, due to the earth abundance of Mg, low cost, reversible H_2 storage capacity, and high energy density, Mg-PMMA nanocomposites are still highly promising and are expected to demonstrate unprecedented performance in storage capacity with further optimization. Mg-PMMA nanocomposites also provide a model system for studying and optimizing air-stable composite materials affording insights that can be translated to other metal hydride and/or nanocomposite systems. For example, despite the vast literature on Mg, systematic studies of Mg nanoparticles in the size range <5 nm remain largely unexplored even though simulations have predicted pronounced effects on nanoparticle energetics for sizes below 1.3 nm.[89] We aim to fill this knowledge gap by generating a library of different sized Mg nanocrystals within the PMMA matrix by modulating the growth at different time points of the reaction. Based on our preliminary results we have laid the groundwork for production of size-controlled air-stable Mg nanocrystals.

Material degradation and poor reversibility are additional challenges with nanoscale Mg since nanoparticles are prone to sintering and/or grain growth over the course of multiple cycles. This is mainly due to the need for ligand removal for efficient H_2 interaction which consequently results in nanoparticle agglomeration and rapid oxidation without the protective capping agents. However, PMMA as a ligand provides a suitable gas-selective matrix and maintains homogenous distribution of the Mg nanocrystals to circumvent these problems. Further, a combination of theory and experiment will enable us to identify a range of optimum matrices with selective H_2 permeability, providing suitable partners for different desired temperature ranges. There are several factors that determine the permeability of polymers including solubility of the molecules composing the polymers, chain packing and side group chemistry, polarity, crystallinity, orientation, and plasticization.[132] Additionally, Fick's law $J = -D\left(\frac{\partial c}{\partial x}\right)$ where J is permeation flux, D is diffusivity and c is concentration of species, enables a crude estimation of the permeability of gases through polymers. Owing to the diverse design rules that make polymers selectively permeable, this gives a broad perspective for polymer chemists to consider: Can we control polymer permeability by altering side chain complexity or chain packing morphology? The ability to modulate these characteristics controllably will open pathways to engineer nanocrystal-polymer nanocomposites with properties that can be tuned with simple synthetic routes.[133]

The kinetics and desorption temperatures of the Mg-PMMA nanocomposites we have reported are compelling; nonetheless, prolific efforts are still needed to enhance these attributes. Introduction of catalysts in the host metal hydride has already been shown to effectively lower desorption temperatures and increase kinetics.[100] However, while catalyst addition can positively tune the properties of the material, it often sacrifices the storage capacity. For example, Pd and Pt are excellent "spill-over" catalysts known to enhance H_2 kinetics by promoting

Downloaded by Lawrence Berkeley National Laboratory on 11 January 2012
Published on 19 October 2011 on http://pubs.rsc.org | doi:10.1039/C1EE02258J

higher concentrations of H_2 dissociation at the surface of the material. However, Pd/Pt catalytic efficiency is accompanied with their high molecular weights which results in overall increased mass and thus loss of H_2 capacity. Nickel (Ni), a 3d transition metal, may offer a better choice as it is comparatively lighter than Pd and Pt, has lower cost, and has been shown to reduce desorption temperature as well as enhance kinetics.[134,135] De Jongh *et al.* recently demonstrated that small amounts of Ni dopants (5–15%) strongly influence the desorption kinetics of Mg. In particular, the overall sample composition controls the dominating phase which either exists as a discrete Mg_2NiH_4-like or a MgH_2-like phase or an intermediate phase when the composition is near the eutectic point ($Mg_{0.88}Ni_{0.12}$).[135] While Mg_2NiH_4 has a lower reversible hydrogen storage capacity (3.6 wt% H_2) relative to MgH_2, we envision that by controllably varying the Ni dopant content in Mg nanocrystals, the kinetics and storage capacity of Mg-PMMA nanocomposites may be improved making them suitable for fuel cells. Further, it will be insightful to determine the role of chemical structuring of these multicomponent alloy nanocrystals in their interaction with H_2. For example, H_2 sorption will be potentially different in nanocrystals with core-shell geometry, *i.e.* with Mg core and Ni shell, relative to when Ni is randomly distributed in the Mg lattice.

The foundational thermodynamic and kinetic properties of Mg-PMMA nanocomposites are yet to be understood, specifically to elucidate the size-dependence of these physical properties. Conventionally, these fundamental characteristics are determined volumetrically by obtaining pressure-composition isotherms using a Sieverts reactor. Gravimetric approaches, such as temperature programmed desorption (TPD) and thermogravimetric analysis (TGA), and crystallographic techniques such as X-ray diffraction are other methods which are commonly adopted as well. While these methods have generated a wealth of information over the past few decades, there are also several drawbacks associated with them which may explain the lack of complete information in the literature of individual nanoscale systems. Very few studies report all of the properties (thermodynamics, kinetics, desorption temperature, H_2 weight percent, scalability and reversibility) required to comprehend the full potential of a system for practical applications. Recently optical methodologies including Raman spectroscopy,[136] modifications in transmission response/reflectivity[137] and alterations in the surface plasmon resonance[138] have enabled rapid determination of metal to metal hydride phase transitions and energies associated with this transformation. Optical techniques circumvent many of the challenges of the aforementioned traditional techniques and facilitate characterization of both nanoparticles and thin films. We aim to explore the properties of Mg-PMMA nanocomposites both by volumetric/gravimetric methods and optical routes to provide a comprehensive understanding of all of its fundamental properties, and how material size and morphology impact performance. Since PMMA is optically silent in the visible and near-infrared, we expect that a transmission/reflectivity study of Mg nanocrystals converting to MgH_2 will allow us to better understand the dynamics of these phase transformations. In particular, understanding size-dependent nucleation energies of the hydride phase by a rapid optical approach would be of critical importance to compare with bulk Mg behavior. Moreover Mg-PMMA nanocomposites would not require palladium (Pd) capping, often used for oxidative stability of Mg, thus eliminating complicated strain effects arising at Mg/Pd interfaces.[139]

Understanding these fundamental material properties is essential for ultimately designing Mg nanocomposite fuel cells. Hydrogen-powered buses have already been successful in Germany and Japan with prototype cars currently being tested.[140] Research is in progress to construct metal hydride fuel cells[39,141] and hybrid fuel cell-batteries[41] which simultaneously performs as a secondary battery when the cells are charged and as a fuel cell when the cells are discharged. Recently, a hybrid fuel cell/battery/electric canal boat was designed and metal hydrides were shown to effectively store 4 kg of H_2 with appropriate desorption rate and temperature suitable for the operation of a 1 kW PEM fuel cell.[142] MgH_2 was also incorporated as a negative electrode in Li-ion batteries, a remarkable example of "cross-fertilization" between battery technology and fuel cells.[40] A small–scale prototype MgH_2 tank was also designed with ball-milled MgH_2 and showed promising initial results of reasonable kinetics and heat and mass transfer in the tank.[143] Given the success of these preliminary studies and the promise of nanoscience, the use of Mg-PMMA designer nanocomposites in fuel cells and hybrid devices can be realistically envisioned. Furthermore, with technological expansion in the last decade in on-chip devices[144] and on-chip power sources such as micro-fuel cells[145] and micro-batteries[146] we foresee the use of Mg-PMMA nanocomposites in such applications and integrated on flexible substrates to develop "bendable fuel cells".[147]

6. Summary

Significant progress has been made thus far in metal hydrides, specifically magnesium hydrides, an important candidate material for H_2-driven fuel cells. Various strategies have been adopted within the past decade to improve the properties of metal hydrides including nanosizing the metal crystals, nanoconfinement in porous carbon frameworks and chemical modifications by doping with metal catalysts or mixing additives of other hydrides. In particular, nanoscale magnesium for hydrogen storage has emerged as a promising storage medium, although many milestones remain to be achieved, such as further reducing the size of Mg nanocrystals to <1 nm, before the full potential of nanosizing is realized. In this context, nanocomposites of hydrogen storage materials in various matrices have begun to receive attention for their enhanced storage properties. One such nanocomposite, Mg nanocrystals in a poly(methyl methacrylate) matrix (Mg-PMMA), has been highlighted as a remarkably promising candidate for addressing some of the current challenges of H_2 storage materials. Finally, there is much potential for future work to be done to improve the material properties of these novel nanocomposites and to explore the fundamental physical properties which contribute to the unique capabilities of this class of material.

Acknowledgements

Work at the Molecular Foundry was supported by the Office of Science, Office of Basic Energy Sciences, at the U.S. Department of Energy under Contract No. DE-AC02-05CH11231. R.B. is

 This journal is © The Royal Society of Chemistry 2011

supported under the US Department of Energy Hydrogen Storage Program. A.M.R. is supported as part of the Center for Nanoscale Control of Geologic CO2, an Energy Frontier Research Center funded by the U.S. Department of Energy, Office of Science, Office of Basic Energy Sciences under Contract No. DE-AC02-05CH11231.

References

1 J. Ausubel, *Am. Sci.*, 1996, **84**, 166–178.
2 J. H. Ausubel, *APPEA J.*, 2007, **2**, 487–495.
3 A. S. Arico, P. Bruce, B. Scrosati, J.-M. Tarascon and W. V. Schalkwijk, *Nat. Mater.*, 2005, **4**, 366–377.
4 C. Liu, F. Li, L.-P. Ma and H.-M. Cheng, *Adv. Mater.*, 2010, **22**, E28–E62.
5 A. Magasinski, P. Dixon, B. Hertzberg, A. Kvit, J. Ayala and G. Yushin, *Nat. Mater.*, 2010, **9**, 353–358.
6 H. Zhang, X. Yu and P. V. Braun, *Nat. Nanotechnol.*, 2011, **6**, 277–281.
7 J.-M. Tarascon, *Philos. Trans. R. Soc. London, Ser. A*, 2010, **368**, 3227–3241.
8 F.-F. Cao, Y.-G. Guo and L.-J. Wan, *Energy Environ. Sci.*, 2011, **4**, 1634–1642.
9 J.-M. Tarascon and M. Armand, *Nature*, 2001, **414**, 359–367.
10 C. Koenigsmann and S. S. Wong, *Energy Environ. Sci.*, 2011, **4**, 1161–1176.
11 R. Devanathan, *Energy Environ. Sci.*, 2008, **1**, 101–119.
12 S. K. Kamarudin, F. Achmad and W. R. W. Daud, *Int. J. Hydrogen Energy*, 2009, **34**, 6902–6916.
13 K. A. Mauritz and R. B. Moore, *Chem. Rev.*, 2004, **104**, 4535–4585.
14 L. Barreto, A. Makihira and K. Riahi, *Int. J. Hydrogen Energy*, 2003, **28**, 267–284.
15 M. Z. Jacobson, W. G. Colella and D. M. Golden, *Science*, 2005, **308**, 1901–1905.
16 A. Züttel, *Mater. Today*, 2003, **6**, 24–33.
17 L. Schlapbach and A. Züttel, *Nature*, 2001, **414**, 353–358.
18 J. Graetz, *Chem. Soc. Rev.*, 2009, **38**, 73–82.
19 U. Eberle, M. Felderhoff and F. Schuth, *Angew. Chem., Int. Ed.*, 2009, **48**, 6608–6630.
20 M. Grätzel, *Nature*, 2001, **414**, 338–344.
21 S. W. Kohl, L. Weiner, L. Schwartsburd, L. Konstantinovski, L. J. W. Shimon, Y. Ben-David, M. A. Iron and D. Milstein, *Science*, 2009, **324**, 74–77.
22 S. W. Boettcher, E. L. Warren, M. C. Putnam, E. A. Santori, D. Turner-Evans, M. D. Kelzenberg, M. G. Walter, J. R. McKone, B. S. Brunschwig, H. A. Atwater and N. S. Lewis, *J. Am. Chem. Soc.*, 2011, **133**, 1216–1219.
23 I. J. Iwuchukwu, M. Vaughn, N. Myers, H. O'Neill, P. Frymier and B. D. Bruce, *Nat. Nanotechnol.*, 2009, **5**, 73–79.
24 A. Paracchino, V. Laporte, K. Sivula, M. Grätzel and E. Thimsen, *Nat. Mater.*, 2011, **10**, 456–461.
25 M. Hambourger, M. Gervaldo, D. Svedruzic, P. W. King, D. Gust, M. Ghirardi, A. L. Moore and T. A. Moore, *J. Am. Chem. Soc.*, 2008, **130**, 2015–2022.
26 A. L. Goff, V. Artero, B. Jousselme, P. D. Tran, N. Guillet, R. Métayé, A. Fihri, S. Palacin and M. Fontecave, *Science*, 2009, **326**, 1384–1387.
27 Y. Hou, B. L. Abrams, P. C. K. Vesborg, M. E. Björketun, K. Herbst, L. Bech, A. M. Setti, C. D. Damsgaard, T. Pedersen, O. Hansen, J. Rossmeisl, S. Dahl, J. K. Nørskov and I. Chorkendorff, *Nat. Mater.*, 2011, **10**, 434–438.
28 C. Weidenthaler and M. Felderhoff, *Energy Environ. Sci.*, 2011, **4**, 2495–2502.
29 J. L. C. Rowsell and O. M. Yaghi, *Angew. Chem., Int. Ed.*, 2005, **44**, 4670–4679.
30 Y. Yürüma, A. Taralpa and T. N. Veziroglu, *Int. J. Hydrogen Energy*, 2009, **34**, 3784–3798.
31 Z. Yang, Y. Xia and R. Mokaya, *J. Am. Chem. Soc.*, 2007, **129**, 1673–1679.
32 N. L. Rosi, J. Eckert, M. Eddaoudi, D. T. Vodak, J. Kim, M. O'Keeffe and O. M. Yaghi, *Science*, 2003, **300**, 1127–1129.
33 X. Zhao, B. Xiao, A. J. Fletcher, K. M. Thomas, D. Bradshaw and M. J. Rosseinsky, *Science*, 2004, **306**, 1012–1015.
34 N. B. McKeown and P. M. Budd, *Chem. Soc. Rev.*, 2006, **35**, 675–683.
35 P. M. Budd, A. Butler, J. Selbie, K. Mahmood, N. B. McKeown, B. Ghanem, K. Msayi, D. Book and A. Walton, *Phys. Chem. Chem. Phys.*, 2007, **9**, 1802–1808.
36 J. Sculley, D. Yuan and H.-C. Zhou, *Energy Environ. Sci.*, 2011, **4**, 2721–2735.
37 *DOE Office of Energy Efficiency and Renewable Energy* (*EERE*). 2009, http://www1.eere.energy.gov/hydrogenandfuelcells/mypp/pdfs/storage.pdf.
38 T. Ho and V. Karri, *Int. J. Hydrogen Energy*, 2010, **35**, 10004–10012.
39 V. C. Y. Kong, F. R. Foulkes, D. W. Kirk and J. T. Hinatsu, *Int. J. Hydrogen Energy*, 1999, **24**, 665–675.
40 Y. Oumellal, A. Rougier, G. A. Nazri, J.-M. Tarascon and L. Aymard, *Nat. Mater.*, 2008, **7**, 916–921.
41 B. Choi, S. Lee, H. Kawai, C. Fushimi and A. Tsutsumi, *Int. J. Hydrogen Energy*, 2009, **34**, 2058–2061.
42 T. K. Mandal and D. H. Gregory, *Annu. Rep. Prog. Chem., Sect. A*, 2009, **105**, 21–54.
43 B. Sakintuna, F. Lamari-Darkrim and M. Hirscher, *Int. J. Hydrogen Energy*, 2007, **32**, 1121–1140.
44 M. U. Niemann, S. S. Srinivasan, A. R. Phani, A. Kumar, D. Y. Goswami and E. K. Stefanakos, *Journal of Nanomaterials*, 2008, 950967.
45 D. R. Paul and L. M. Robeson, *Polymer*, 2008, **49**, 3187–3204.
46 A. C. Balazs, T. Emrick and T. P. Russell, *Science*, 2006, **314**, 1107–1110.
47 P. E. d. Jongh and P. Adelhelm, *Chem. Sus. Chem.*, 2010, **3**, 1332–1348.
48 V. Berube, G. Radtke, M. Dresselhaus and G. Chen, *Int. J. Energy Res.*, 2007, **31**, 637–663.
49 K. C. Kim, B. Dai, J. K. Johnson and D. S. Sholl, *Nanotechnology*, 2009, **20**, 204001.
50 K.-F. Aguey-Zinsou and J.-R. Ares-Fernández, *Energy Environ. Sci.*, 2010, **3**, 526–543.
51 K.-J. Jeon, H. R. Moon, A. M. Ruminski, B. Jiang, C. Kisielowski, R. Bardhan and J. J. Urban, *Nat. Mater.*, 2011, **10**, 286–290.
52 L. George and S. K. Saxena, *Int. J. Hydrogen Energy*, 2010, **35**, 5454–5470.
53 J. J. Vajo, S. L. Skeith and F. Mertens, *J. Phys. Chem. B*, 2005, **109**, 3719–3722.
54 T. K. Nielsen, U. Bösenberg, R. Gosalawit, M. Dornheim, Y. Cerenius, F. Besenbacher and T. R. Jensen, *ACS Nano*, 2010, **4**, 3903–3908.
55 A. F. Gross, J. J. Vajo, S. L. V. Atta and G. L. Olson, *J. Phys. Chem. C*, 2008, **112**, 5651–5657.
56 M. Christian and K.-F. Aguey-Zinsou, *Nanoscale*, 2010, **2**, 2587–2590.
57 Y. Zhang, W.-S. Zhang, Ai-Qin. Wang, L.-X. Sun, M.-Q. Fan, H.-L. Chu, J.-C. Sun and T. Zhang, *Int. J. Hydrogen Energy*, 2007, **32**, 3976–3980.
58 O. Friedrichs, J. W. Kim, A. Remhof, F. Buchter, A. Borgschulte, D. Wallacher, Y. W. Cho, M. Fichtner, K. H. Oh and A. Züttela, *Phys. Chem. Chem. Phys.*, 2009, **11**, 1515–1520.
59 P.-J. Wang, Z.-Z. Fang, L.-P. Ma, X.-D. Kang and P. Wang, *Int. J. Hydrogen Energy*, 2008, **33**, 5611–5616.
60 E. G. Bardají, Z. Zhao-Karger, N. Boucharat, A. Nale, M. J. v. Setten, W. Lohstroh, E. Röhm, M. Catti and M. Fichtner, *J. Phys. Chem. C*, 2011, **115**, 6095–6101.
61 Y. Zhang, W.-S. Zhang, A.-Q. Wang, L.-X. Sun, M.-Q. Fan, H.-L. Chu, J.-C. Sun and T. Zhang, *Int. J. Hydrogen Energy*, 2007, **32**, 3976–3398.
62 C. P. Balde, B. P. C. Hereijgers, J. H. Bitter and K. P. d. Jong, *J. Am. Chem. Soc.*, 2008, **130**, 6761–6765.
63 T. Mueller and G. Ceder, *ACS Nano*, 2010, **4**, 5647–5656.
64 W. Lohstroh, A. Roth, H. Hahn and M. Fichtner, *ChemPhysChem*, 2010, **11**, 789–792.
65 J. Gao, P. Adelhelm, M. H. W. Verkuijlen, C. Rongeat, M. Herrich, P. J. M. v. Bentum, O. Gutfleisch, A. P. M. Kentgens, K. P. d. Jong and P. E. d. Jongh, *J. Phys. Chem. C*, 2010, **114**, 4675–4682.
66 R. K. Bhakta, J. L. Herberg, B. Jacobs, A. Highley, R. Behrens, N. W. Ockwig, J. A. Greathouse and M. D. Allendorf, *J. Am. Chem. Soc.*, 2009, **131**, 13198–13199.
67 P. Wang and C. M. Jensen, *J. Phys. Chem. B*, 2004, **108**, 15827–15829.

Downloaded by Lawrence Berkeley National Laboratory on 11 January 2012
Published on 19 October 2011 on http://pubs.rsc.org | doi:10.1039/C1EE02258J

Downloaded by Lawrence Berkeley National Laboratory on 11 January 2012
Published on 19 October 2011 on http://pubs.rsc.org | doi:10.1039/C1EE02258J

68 X. Xiao, X. Fan, K. Yu, S. Li, C. Chen, Q. Wang and L. Chen, *J. Phys. Chem. C*, 2009, **113**, 20745–20751.
69 P. A. Berseth, A. G. Harter, R. Zidan, A. Blomqvist, C. M. s. A. jo, R. H. Scheicher, R. Ahuja and P. Jena, *Nano Lett.*, 2009, **9**, 1501–1505.
70 A. W. Vittetoe, M. U. Niemann, S. S. Srinivasan, K. McGrath, A. Kumar, D. Y. Goswami, E. K. Stefanakos and S. Thomas, *Int. J. Hydrogen Energy*, 2009, **34**, 2333–2339.
71 J. Graetz, J. Wegrzyn and J. J. Reilly, *J. Am. Chem. Soc.*, 2008, **130**, 17790–17794.
72 C. Weidenthaler, A. Pommerin, M. Felderhoff, W. Sun, C. Wolverton, B. Bogdanović and F. Schüth, *J. Am. Chem. Soc.*, 2009, **131**, 16735–16743.
73 T. Umegaki, J.-M. Yan, X.-B. Zhang, H. Shioyama, N. Kuriyama and Q. Xu, *Int. J. Hydrogen Energy*, 2009, **34**, 2303–2311.
74 B. Peng and J. Chen, *Energy Environ. Sci.*, 2008, **1**, 479–483.
75 C. W. Hamilton, R. T. Baker, A. Staubitz and I. Manners, *Chem. Soc. Rev.*, 2009, **38**, 279–293.
76 U. B. Demirci and P. Miele, *Energy Environ. Sci.*, 2009, **2**, 627–637.
77 A. Gutowska, L. Li, Y. Shin, C. M. Wang, X. S. Li, J. C. Linehan, R. S. Smith, B. D. Kay, B. Schmid, W. Shaw, M. Gutowski and T. Autrey, *Angew. Chem., Int. Ed.*, 2005, **44**, 3578–3582.
78 A. Feaver, S. Sepehri, P. Shamberger, A. Stowe, T. Autrey and G. Cao, *J. Phys. Chem. B*, 2007, **111**, 7469–7472.
79 J.-M. Yan, X.-B. Zhang, S. Han, H. Shioyama and Q. Xu, *Inorg. Chem.*, 2009, **48**, 7389–7393.
80 O. Metin, V. Mazumder, S. Ozkar and S. Sun, *J. Am. Chem. Soc.*, 2010, **132**, 1468–1469.
81 S. B. Kalidindi, U. Sanyal and B. R. Jagirdar, *Phys. Chem. Chem. Phys.*, 2008, **10**, 5870–5874.
82 H.-L. Jiang, T. Umegaki, T. Akita and X.-B. Zhang, *Chem.–Eur. J.*, 2010, **16**, 3132–3137.
83 J.-M. Yan, X.-B. Zhang, T. Akita, M. Haruta and Q. Xu, *J. Am. Chem. Soc.*, 2010, **132**, 5326–5327.
84 D. Neiner, A. Karkamkar, J. C. Linehan, B. Arey, T. Autrey and S. M. Kauzlarich, *J. Phys. Chem. C*, 2009, **113**, 1098–1103.
85 Y. S. Chua, P. Chen, G. Wu and Z. Xiong, *Chem. Commun.*, 2011, **47**, 5116–5129.
86 Z. Xiong, C. K. Yong, G. Wu, P. Chen, W. Shaw, A. Karkamkar, T. Autrey, M. O. Jones, S. R. Johnson, P. P. Edwards and W. I. F. David, *Nat. Mater.*, 2007, **7**, 138–141.
87 Z. Xiong, Y. S. Chua, G. Wu, W. Xu, P. Chen, W. Shaw, A. Karkamkar, J. Linehan, T. Smurthwaite and T. Autrey, *Chem. Commun.*, 2008, 5595–5597.
88 J. F. Stampfer, C. E. Holley and J. F. Suttle, *J. Am. Chem. Soc.*, 1960, **82**, 3504–3508.
89 R. W. P. Wagemans, J. H. v. Lenthe, P. E. d. Jongh, A. J. v. Dillen and K. P. d. Jong, *J. Am. Chem. Soc.*, 2005, **127**, 16675–16680.
90 Z. Wu, M. D. Allendorf and J. C. Grossman, *J. Am. Chem. Soc.*, 2009, **131**, 13918–13919.
91 K. C. Smith, T. S. Fisher, U. V. Waghmare and R. Grau-Crespo, *Phys. Rev. B: Condens. Matter Mater. Phys.*, 2010, **82**, 134109.
92 M. Pozzo and D. Alfe, *Int. J. Hydrogen Energy*, 2009, **34**, 1922–1930.
93 S. Er, G. A. d. Wijs and G. Brocks, *J. Phys. Chem. Lett.*, 2010, **1**, 1982–1986.
94 P. Vermeulen, E. F. M. J. v. Thiel and P. H. L. Notte, *Chem.–Eur. J.*, 2007, **13**, 9892–9898.
95 S. V. Alapati, J. K. Johnson and D. S. Sholl, *J. Phys. Chem. C*, 2007, **111**, 1584–1591.
96 A. J. Du, S. C. Smith, X. D. Yao and G. Q. Lu, *J. Am. Chem. Soc.*, 2007, **129**, 10201–10204.
97 S. Agarwal, A. Aurora, A. Jain, I. P. Jain and A. Montone, *Int. J. Hydrogen Energy*, 2009, **34**, 9157–9162.
98 N. Bazzanella, R. Checchetto, A. Miotello, C. Sada, P. Mazzoldi and P. Mengucci, *Appl. Phys. Lett.*, 2006, **89**, 014101.
99 E. Callini, L. Pasquini, L. H. Rude, T. K. Nielsen, R. Jensen and E. Bonetti, *J. Appl. Phys.*, 2010, **108**, 073513.
100 N. Hanada, T. Ichikawa and H. Fujii, *J. Phys. Chem. B*, 2005, **109**, 7188–7194.
101 J. Lu, Y. J. Choi, Z. Z. Fang, H. Y. Sohn and E. Ronnebro, *J. Am. Chem. Soc.*, 2009, **131**, 15843–15852.
102 R. A. Varin, Z. Zaranski, T. Czujko, M. Polanski and Z. S. Wronski, *Int. J. Hydrogen Energy*, 2011, **36**, 1177–1183.
103 F. Dolci, M. D. Chio, M. Baricco and E. Giamello, *Mater. Res. Bull.*, 2009, **44**, 194–197.
104 I. E. Malka, T. Czujko and J. Bystrzycki, *Int. J. Hydrogen Energy*, 2010, **35**, 1706–1712.
105 J. J. Vajo, F. Mertens, C. C. Ahn, R. C. Bowman and B. Fultz, *J. Phys. Chem. B*, 2004, **108**, 13977–13983.
106 L. L. Shaw, X. Wan, J. Z. Hu, J. H. Kwak and Z. Yang, *J. Phys. Chem. C*, 2010, **114**, 8089–8098.
107 J. Yang, A. Sudik, D. J. Siegel, D. Halliday, A. Drews, R. O. Carter, C. Wolverton, G. J. Lewis, J. W. A. Sachtler, J. J. Lo, S. A. Faheem, D. A. Lesch and V. Ozolins, *Angew. Chem., Int. Ed.*, 2008, **47**, 882–887.
108 M. Tanniru, D. K. Slattery and F. Ebrahimi, *Int. J. Hydrogen Energy*, 2010, **35**, 3555–3564.
109 M. Paskevicius, D. A. Sheppard and C. E. Buckley, *J. Am. Chem. Soc.*, 2010, **132**, 5077–5083.
110 M. Arrowsmith, M. S. Hill, D. J. MacDougall and M. F. Mahon, *Angew. Chem., Int. Ed.*, 2009, **48**, 4013–4016.
111 S. Harder, J. Spielmann, J. Intemann and H. Bandmann, *Angew. Chem., Int. Ed.*, 2011, **50**, 4156–4160.
112 K.-F. Aguey-Zinsou and J.-R. Ares-Fernández, *Chem. Mater.*, 2008, **20**, 376–378.
113 S. B. Kalidindi and B. R. Jagirdar, *Inorg. Chem.*, 2009, **48**, 4524–4529.
114 N. S. Norberg, T. S. Arthur, S. J. Fredrick and A. L. Prieto, *J. Am. Chem. Soc.*, 2011, **133**, 10679–10681.
115 I. Haas and A. Gedanken, *Chem. Commun.*, 2008, 1795–1797.
116 W. Li, C. Li, H. Ma and J. Chen, *J. Am. Chem. Soc.*, 2007, **129**, 6710–6711.
117 S. Barcelo, M. Rogers, C. P. Grigoropoulos and S. S. Mao, *Int. J. Hydrogen Energy*, 2010, **35**, 7232–7235.
118 H. Imamura, Y. Usui and M. Takashima, *J. Less Common Met.*, 1991, **175**, 171–176.
119 L. Li, B. Peng, W. Ji and J. Chen, *J. Phys. Chem. C*, 2009, **113**, 3007–3013.
120 R. K. Singh, H. Raghubanshi, S. K. Pandey and O. N. Srivastava, *Int. J. Hydrogen Energy*, 2010, **35**, 4131–4137.
121 A. D. Rud, A. M. Lakhnik, V. G. Ivanchenko, V. N. Uvarov, A. A. Shkola, V. A. Dekhtyarenko, L. I. Ivaschuk and N. I. Kuskova, *Int. J. Hydrogen Energy*, 2008, **33**, 1310–1316.
122 B. S. Amirkhiz, M. Danaie, M. Barnes, B. Simard and D. Mitlin, *J. Phys. Chem. C*, 2010, **114**, 3265–3275.
123 P. E. d. Jongh, R. W. P. Wagemans, T. M. Eggenhuisen, B. S. Dauvillier, P. B. Radstake, J. D. Meeldijk, J. W. Geus and K. P. d. Jong, *Chem. Mater.*, 2007, **19**, 6052–6057.
124 T. K. Nielsen, K. Manickam, M. Hirscher, F. Besenbacher and T. R. Jensen, *ACS Nano*, 2009, **3**, 3521–3528.
125 A. F. Gross, C. C. Ahn, S. L. V. Atta, P. Liu and J. J. Vajo, *Nanotechnology*, 2009, **20**, 204005.
126 S. Zhang, A. F. Gross, S. L. V. Atta, M. Lopez, P. Liu, C. C. Ahn, J. J. Vajo and C. M. Jensen, *Nanotechnology*, 2009, **20**, 204027.
127 M. Paskevicius, H.-Y. Tian, D. A. Sheppard, C. J. Webb, M. P. Pitt, E. M. Gray, N. M. Kirby and C. E. Buckley, *J. Phys. Chem. C*, 2011, **115**, 1757–1766.
128 P. Adelhelm and P. E. d. Jongh, *J. Mater. Chem.*, 2011, **21**, 2417–2427.
129 H.-J. Liu, J. Yip and K.-S. Shia, *Tetrahedron Lett.*, 1997, **38**, 2253–2256.
130 R. D. Rieke, *Science*, 1989, **246**, 1260–1264.
131 P. S. Rudman, *J. Appl. Phys.*, 1979, **50**, 7195–7199.
132 B. D. Freeman and I. Pinnau, *Polymer Membranes for Gas and Vapor Separation: Chemistry and Materials Science*, ACS Publication Inc., Washington DC, 1999.
133 G. Odian, *Principles of Polymerization*, John Wiley & Sons Inc., New York, 2004.
134 A. Zaluska, L. Zaluski and J. O. Strom-Olsen, *J. Alloys Compd.*, 1999, **289**, 197–206.
135 R. e. Bogerd, P. Adelhelm, J. H. Meeldijk, K. P. d. Jong and P. E. d. Jongh, *Nanotechnology*, 2009, **20**, 204019.
136 J. F. Li, Y. F. Huang, Y. Ding, Z. L. Yang, S. Bo, X. S. Zhou, F. R. Fan, W. Zhang, Z. Y. Zhou, D. Y. Wu, B. Ren, Z. L. Wang and Z. Q. Tian, *Nature*, 2010, **464**, 392–395.
137 R. Gremaud, M. Slaman, H. Schreuders, B. Dam and R. Griessen, *Appl. Phys. Lett.*, 2007, **91**, 231916.
138 N. Liu, M. L. Tang, M. Hentschel, H. Giessen and A. P. Alivisatos, *Nat. Mater.*, 2011, **10**, 631–636.
139 A. Baldi, M. Gonzalez-Silveira, V. Palmisano, B. Dam and R. Griessen, *Phys. Rev. Lett.*, 2009, **102**, 226102.

 This journal is © The Royal Society of Chemistry 2011

View Online

140 L. Schlapbach, *Nature*, 2009, **460**, 809–810.
141 V. C. Y. Kong, D. W. Kirk, F. R. Foulkes and J. T. Hinatsu, *Int. J. Hydrogen Energy*, 2003, **28**, 205–214.
142 A. I. Bevan, A. Zuttel, D. Book and I. R. Harris, *Faraday Discuss.*, 2011, **151**, 353–367, DOI: 10.1039/C0FD00025F.
143 A. Chaise, P. d. Rango, P. Marty and D. Fruchart, *Int. J. Hydrogen Energy*, 2010, **35**, 6311–6322.
144 D. Tham and J. R. Heath, *Nano Lett.*, 2010, **10**, 4429–4434.
145 S. Tominaka, H. Nishizeko, S. Ohta and T. Osaka, *Energy Environ. Sci.*, 2009, **2**, 849–852.
146 H. Nakano, K. Dokko, J.-i. Sugaya, T. Yasukawa, T. Matsue and K. Kanamura, *Electrochem. Commun.*, 2007, **9**, 2013–2017.
147 S. Tominaka, H. Nishizeko, J. Mizuno and T. Osaka, *Energy Environ. Sci.*, 2009, **2**, 1074–1077.

Downloaded by Lawrence Berkeley National Laboratory on 11 January 2012
Published on 19 October 2011 on http://pubs.rsc.org | doi:10.1039/C1EE02258J